INTERNATIONAL JOURNAL OF INTEGRATED ENGINEERING
ISSN: 2229-838X e-ISSN: 2600-7916

IJIE

Vol. 16 No. 5 (2024) 466-475
https://publisher.uthm.edu.my/ojs/index.php/ijie

Experimental Investigation of a Novel CFRP-Steel Composite Tube-Confined Seawater-Sea Sand Concrete Intermediate Long Column

Hao Fu[1], Kangle Guo[2], Zhaojun Wu[2], Rihao Mai[1], Chee-Loong Chin[1]*, Chau-Khun Ma[1]

[1] *Department of Structures and Materials, Faculty of Civil Engineering, Universiti Teknologi Malaysia, 81300 Skudai, Johor, MALAYSIA*
[2] *School of Civil Engineering, Jiangxi University of Engineering, Xinyu, 338000, CHINA*

*Corresponding Author: cheeloong.chin@utm.my
DOI: https://doi.org/10.30880/ijie.2024.16.05.035

Article Info

Received: 15 March 2024
Accepted: 12 August 2024
Available online: 29 August 2024

Keywords

CFRP, seawater-sea sand concrete, axial compression, ultimate load bearing capacity, confinement

Abstract

In order to fully utilize sea sand in offshore engineering, a novel carbon fiber-reinforced polymer (CFRP)-steel composite tube-confined seawater-sea sand concrete (FCTSSC) column structure has been developed. This study conducts experimental investigations on FCTSSC intermediate long columns for the first time. It investigates the failure modes and the impact of the external CFRP layers number on the axial compression performance. The results reveal that the FCTSSC intermediate long column specimens exhibit the failure modes of global buckling and localized steel tube bulging. After CFRP restriction, the ultimate load bearing capacity of the specimens increased from 12.51% to 20.87%. The ultimate load bearing capacity, its enhancement percentage, and peak lateral deformation are all positively correlated with the external CFRP layers number. Finally, a summary and assessment were conducted on the applicability and accuracy of the existing load bearing capacity models, providing a reference for subsequent research.

1. Introduction

As maritime development continues to advance worldwide, large-scale construction of offshore projects requires substantial concrete usage. In offshore engineering construction, using local seawater and sea sand resources can be allowed for on-site sourcing. This can significantly reduce the material transportation costs compared with the river water and river sand [1]-[5].

Fiber-reinforced polymer (FRP) has several advantages, including lightweight, excellent strength, anti-corrosion properties, and ease of construction [6]-[9]. In 2011, Teng et al. [10] first proposed the design concept of combining FRP and SSC. Since then, it has been found that this combination can improve the mechanical performance [11], [12] and durability [13]-[15] in short-term or long-term structural applications. CFST structures are widely used in the field of civil engineering. To prevent chloride ions in SSC from corroding the steel tube, stainless steel tubes have been used in combination with SSC and perform good mechanical properties [16], [17]. However, stainless steel tubes are expensive and prone to outward buckling. This has become a bottleneck for their widespread application in offshore engineering.

To overcome these drawbacks, Wei et al. [18] introduced a novel FCTSSC column structure based on the FCFST structure. A schematic diagram of this structure is shown in Fig. 1. This structure utilizes FRP fabric pasted

on the inner and outer walls of the steel tube. The composite tube is filled with SSC. This structure overcoming the drawback of corrosion on the internal wall of the steel pipe. Additionally, it enhances the mechanical performance of the component. Wei et al. [18] experimental research indicates that the internal and external FRP can significantly improve the ultimate load bearing capacity and deformation capability. Subsequently, Wei et al. [19] conducted experimental research on novel FCTSSC columns, which filled with high-strength seawater-sea sand concrete. The results revealed that the CFRP composite specimens exhibited a higher ultimate load bearing capacity compared to basalt fiber-reinforced polymer (BFRP) composite specimens. Additionally, they proposed a stress-strain curve prediction model for that. Wang et al. [20] produced a novel FCTSSC column made of seawater-sea sand-coral concrete. It demonstrated that the mechanical performance of the components increased as the number of CFRP layers increased. However, the effect of the steel tube diameter-to-thickness ratio was the opposite. Zhang et al. [21] conducted cyclic axial compression tests on these novel FCTSSC columns. It showed that FRP can effectively restrict the lateral expansion of SSC and proposed a more rational cyclic stress-strain model. Huang et al. [22] tested the mechanical behavior of FCTSSC short columns made of CFRP. It studied the effects of steel tube wall thickness, steel tube yield strength, CFRP layer number and position, and concrete strength. They also discussed the applicability of existing models for bearing capacity calculations.

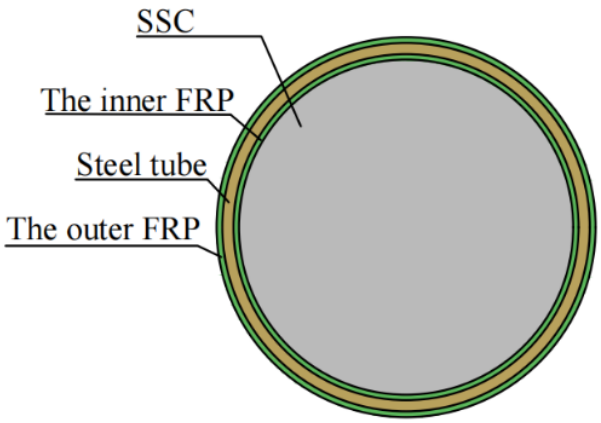

Fig. 1 *Structure diagram of the FCTSSC column*

Evidently, the research scope of this novel FCTSSC column structure has significant limitations. Previous research only focused on short columns. Therefore, this paper conducts experimental research on FCTSSC intermediate long columns for the first time. The aim is to comprehend their failure modes and analyze the impact of external CFRP layers number on their axial compression performance. This can serve as a reference for future research and application.

2. Test Program

2.1 Specimens Design

A total of four axial compression specimens were designed for this experiment. It includes three FCTSSC columns and one seawater-sea sand concrete filled steel tube (SFST) column. The SFST column was served as the control specimen. The experimental parameter was the external CFRP layers number. Table 1 provides the parameters detail for all specimens. Among these, SC24 represents the SFST column specimen with a slenderness ratio of 16.8. CF1SC24, CF2SC24, and CF3SC24 represent the FCTSSC intermediate long column specimen with a slenderness ratio of 16.8 and contain 1, 2, and 3 external CFRP layers, respectively.

2.2 Material Properties

In this experiment, the material properties of the steel tube were tested. Its yield strength is 313.2 MPa, ultimate tensile strength is 485.5 MPa, and elastic modulus is 200.4 GPa. The mechanical properties of the CFRP fabric used in this study were provided by the manufacturer. It has an ultimate tensile strength of 3216.0 MPa, elastic modulus of 210.0 MPa, and ultimate tensile strain of 0.017. The SSC mix proportions listed in Table 2 for this experiment were designed in accordance with the standard JGJ55-2011 [23]. Ordinary Portland cement with a strength grade of 42.5 MPa was used, along with fine aggregate consisting of well-graded sea sand from Rizhao, Shandong, China. Crushed granite with a nominal size of 20 mm is used as coarse aggregates. The composition of seawater is tabulated in Table 3 in accordance with ASTM D1141-98 [24]. The compressive strength test measured the compressive strength and elastic modulus of the SSC cylinder as 33.1 MPa and 27.9 GPa, respectively.

Int. Journal of Integrated Engineering Vol. 16 No. 5 (2024) p. 466-475

Table 1 *Parameters of all specimens*

Specimen Identification	Specimen Height, H (mm)	Outer Diameter of Steel Tube, D_s (mm)	Thickness Of Steel Tube, t_s (mm)	Concrete Strength, f_c (MPa)	Layers of Outer CFRP Fabric, n_f
SC24	960	159	4.5	C40	-
CF1SC24	960	159	4.5	C40	1
CF2SC24	960	159	4.5	C40	2
CF3SC24	960	159	4.5	C40	3

Table 2 *Mix proportions of C40 SSC*

Cement (kg/m³)	Seawater (kg/m³)	Sea Sand (kg/m³)	Coarse Aggregate (kg/m³)
501	220	566	1123

Table 3 *Composition of seawater*

NaCl (kg/m³)	$MgCl_2$ (kg/m³)	Na_2SO_4 (kg/m³)	$CaCl_2$ (kg/m³)	KCl (kg/m³)	$NaHCO_3$ (kg/m³)
24.53	5.20	4.09	1.16	0.695	0.201

2.3 Test Loading and Measurement Program

In this experiment, the specimen fabrication followed the process outlined in Wei et al. [18]. First, use a plastic tube to guide the CFRP fabric to adhere to the inner wall of the steel tube coated with epoxy resin adhesive. Then, roll the steel tube with its outer wall coated with epoxy resin adhesive over the end of the CFRP fabric. It is not proper until the outer wall of the steel tube is completely wrapped. Finally, attach strain gauges, weld wires, and perform concrete casting and curing. The experiment was conducted using a 5000 kN electro-hydraulic servo long column compression testing machine illustrated in Fig. 2(a). The upper loading platen was connected via a ball joint, while the lower loading platen was connected to the hydraulic device. Before the formal testing, the specimens underwent three repeated preloading cycles. During the formal loading stage, displacement-controlled loading was applied with a speed of 0.5 mm/min. The test was terminated when a significant buckling deformation was observed.

The measurement setup for this experiment is shown in Fig. 2(b). Longitudinal and transverse strain gauges are placed on the upper, middle, and lower sections of the outer CFRP layer surface at 90° intervals in the circumferential direction. At the 1/4, 1/2, and 3/4 heights of the specimen, six mutually perpendicular lateral displacement transducers are placed at 90° intervals in the circumferential direction to monitor the lateral deformation. Finally, two longitudinal displacement gauges were symmetrically positioned on each side of the specimen to monitor axial deformation.

3. Results and Discussions

3.1 Failure Mode

Fig. 3(a) illustrates the failure mode of the SC24 specimen. The experiment revealed that SC24 experienced global buckling failure without noticeable bulging on the steel tube surface. As the observed phenomena of FCTSSC specimens were consistent, CF3SC24 was selected to show the failure mode as shown in Fig. 3(b).

During the test, a sharp explosive sound was heard when the load reached its ultimate load bearing capacity. At this point, localized fiber fabric instantaneously ruptured, exhibiting filamentous or banded ruptures. Visible signs of slight bending appeared in the upper part of the specimen, and a sudden drop in the axial load-deformation curve occurred. This abrupt change was due to the instantaneous brittle rupture of the CFRP fabric, leading to the sudden loss of partial restriction. As the loading continued, the area and location of CFRP fabric ruptures gradually increased. After cutting open the CFRP fabric, it was observed that the rupture positions were mostly accompanied by bulging on the steel tube. This phenomenon occurred because these areas lost external CFRP fabric confinement. It caused stress concentration and deformation release. Eventually, the lateral deformation of the specimen became more pronounced. The specimen displayed a failure mode of global buckling accompanied by localized bulging of the steel tube as shown in Fig. 3(c).

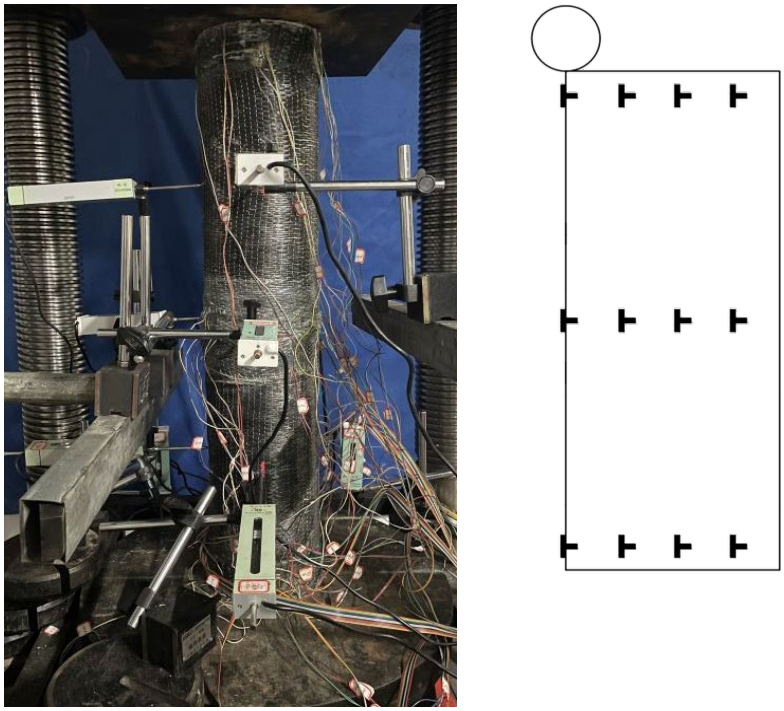

(a) Experimental setup **(b) Strain gauge positioning**

Fig. 2 *Loading device and measuring program*

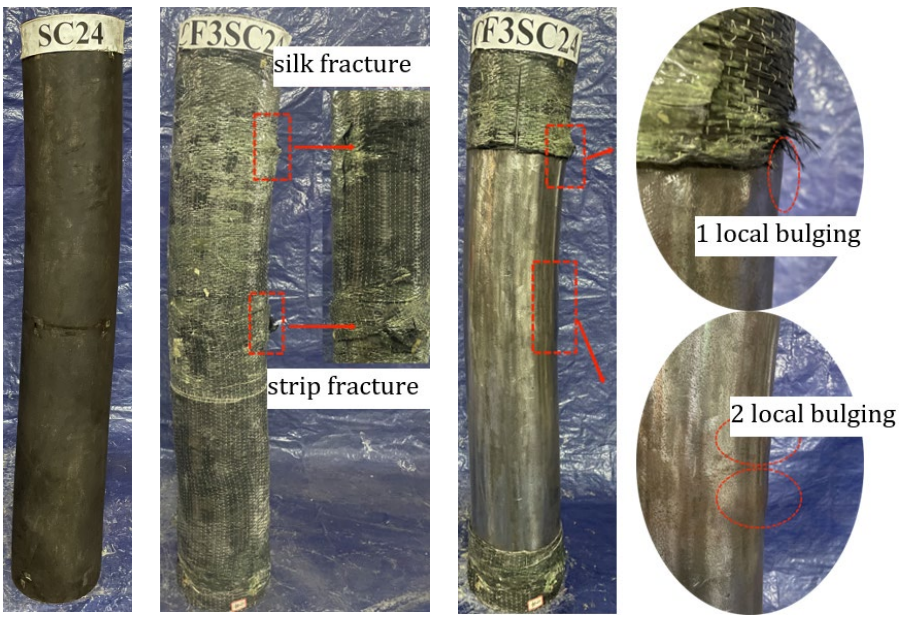

(a) SC24 **(b) CF3SC24** **(c) Local bulging of CF3SC24**

Fig. 3 *Failure mode of specimens*

3.2 Axial Load-Deformation Curve

Fig. 4 illustrates the impact of the external CFRP fabric layers number on the axial load-deformation curve of the FCTSSC columns. It can be found that the external CFRP fabric layers number has minimal impact on the initial axial stiffness of the FCTSSC columns. Conversely, the post-elastic stiffness enhances as the external CFRP fabric layers number increases. This implies that the confinement provided by the external CFRP fabric increases. It also makes the ultimate load bearing capacity increase.

Fig. 5(a) presents the impact of the external CFRP fabric layers number on the ultimate load bearing capacity of FCTSSC columns. It is evident that when the external CFRP layers number increases, the enhancement percentage in the ultimate load bearing capacity decreases. For instance, the ultimate load bearing capacity of

Int. Journal of Integrated Engineering Vol. 16 No. 5 (2024) p. 466-475

CF2SC24 is 5.86% higher than that of CF1SC24, while CF3SC24 is only 1.49% higher than CF2SC24. Fig. 5(b) depicts the impact of the external CFRP layers number on the enhancement percentage of the ultimate load bearing capacity. This percentage is compared between the FCTSSC columns and the SFST column. This reflects the impact of changes in the size of external CFRP fabric confinement on the lifting of ultimate load bearing capacity. It is evident that the enhancement percentage in ultimate load bearing capacity increases when the external CFRP layers number increases. Specimens with 1, 2, and 3 layers show improvements of 12.51%, 19.1%, and 20.87%, respectively. Furthermore, the increase magnitude of the enhancement percentage decreases as the external CFRP layers number increases. For instance, CF2SC24 exhibits an enhancement percentage in ultimate load bearing capacity that is 6.29% higher than CF1SC24, whereas CF3SC24 is only 1.77% higher than CF2SC24. This implies an efficiency limitation of external CFRP fabric usage. That is the effectiveness of CFRP confinement displays a negative correlation trend with the CFRP fabric layers number. In summary, it is recommended that in practical engineering applications, employing 2 layers of external CFRP fabric for FCTSSC intermediate long columns is more economically reasonable.

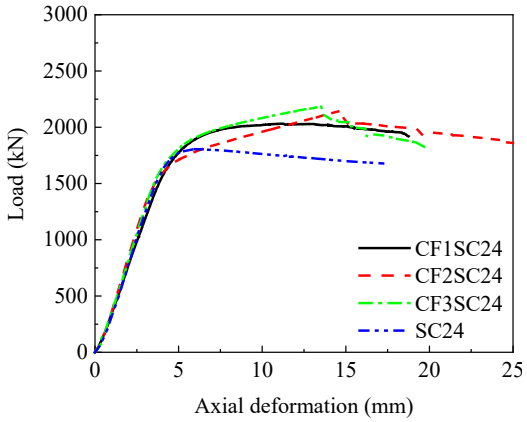

Fig. 4 *Impact of the external CFRP layers number on axial load-deformation curves*

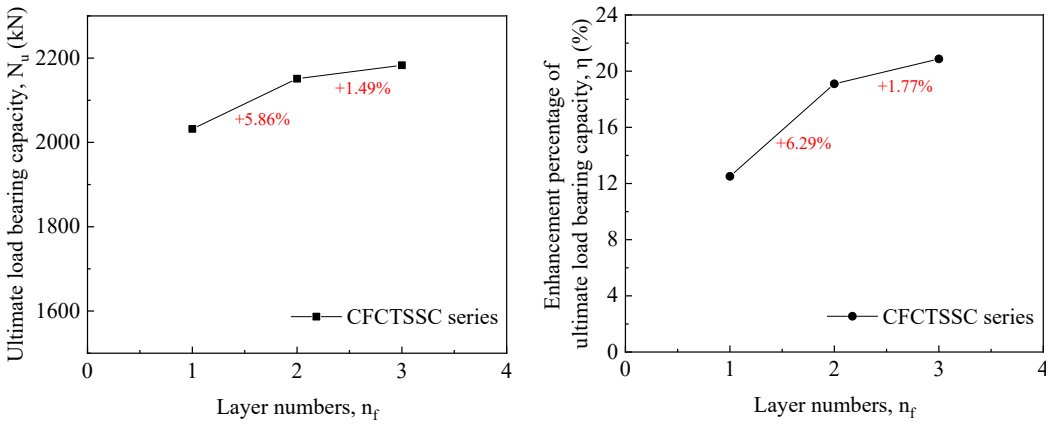

(a) Ultimate load bearing capacity **(b) Enhancement percentage**

Fig. 5 *Impact of external CFRP layer numbers*

3.3 Axial Load-Lateral Deformation Curve

Fig. 6 depicts the axial load-lateral deformation curves under different numbers of external CFRP fabric layers. It is evident that the lateral deformation variation curves at 2/4 and 3/4 heights for all specimens are quite similar. Additionally, the lateral deformation at 3/4 height is consistently larger than those at 2/4 height. This pattern aligns with the main failure mode occurring in the upper-middle portion of the specimens. Notably, due to the relatively low lateral stiffness of the specimens, lateral deformation developed less than 2 mm during the elastic phase. For all specimens, it is observed that lateral deformation starts to increase gradually when the load reaches approximately 80%. This indicates the start of overall instability. As the load increases, the lateral deformation increases rapidly. The FCTSSC columns show good ductility throughout this process. Moreover, the external CFRP fabric layers number has a negligible impact on the initial lateral stiffness of the specimens, whether at 2/4 or 3/4 height.

Fig. 7 quantitatively illustrates the impact of the external CFRP layers number on peak lateral deformation, where δ_u represents the peak lateral deformation. It can be seen that both at 2/4 and 3/4 height, peak lateral

deformation increases as the external CFRP fabric layers number increases. This indicates the confinement effect of the external CFRP fabric enhances the deformation capacity. Specifically, at 2/4 and 3/4 height, the range of peak lateral deformation is 5.62 mm to 6.31 mm and 6.21 mm to 7.75 mm, respectively. Furthermore, the magnitude of increase in peak lateral deformation at 3/4 height is consistently greater than that at 2/4 height. For instance, when the CFRP layers range from 1 to 3, the percentage increase in peak lateral deformation at 2/4 height is 7.1% and 4.82%. However, it is 11.11% and 12.24% at 3/4 height. This is consistent with the primary occurrence of the final failure mode at the 3/4 height of the specimen.

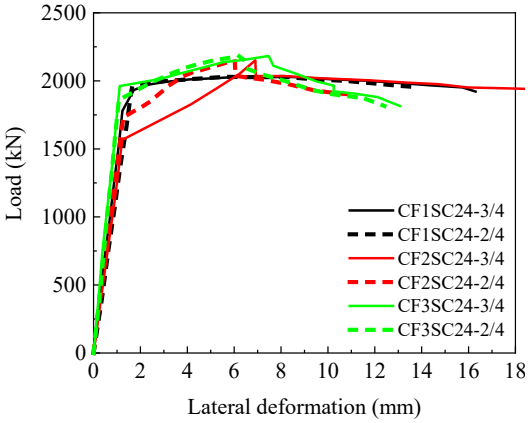

Fig. 6 *Impact of external CFRP layer numbers on axial load-lateral deformation curves*

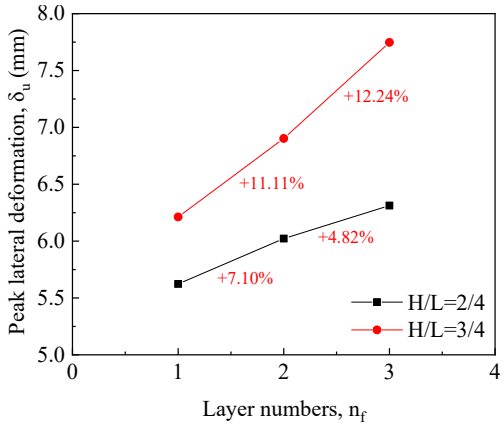

Fig. 7 *Impact of external CFRP layer numbers on peak lateral deformation*

4. Load Bearing Capacity Model Evaluation

Currently, only a limited number of studies have been conducted on FCTSSC short columns, and this paper conducted the first research on immediate long columns. FRP-confined concrete-filled steel tube (FCFST) columns have undergone extensive research. It has structural similarities with FCTSSC, and the key difference lies in the attachment of FRP fabric to the inner surface of FCTSSC columns. Therefore, this paper summarizes the load bearing capacity models for FCFST immediate long columns proposed by various scholars in recent years, followed by analysis and evaluation.

Liu et al. [25] referenced the calculation method for the stable load bearing capacity of concrete-filled steel tube (CFST) columns. They introduced a reduction stability coefficient into the load bearing capacity formula of short column, as shown below:

$$N_{ul} = \varphi N_{us} \tag{1}$$

$$\varphi = 1 - 0.1337\sqrt{L/D - 5.7}, \quad 5.7 \le L/D \le 18 \tag{2}$$

where N_{ul} is the axial-compressed ultimate load bearing capacity of FCFST immediate long columns; φ is the stability coefficient; L is the column length; D is the cross-sectional diameter of the component; N_{us} is the axial-compressed ultimate load bearing capacity of FCFST short columns. The specific calculation method is detailed in literature [25].

Yu et al. [26] proposed that the stability coefficient for the load bearing capacity of FCFST immediate long columns is determined by the stability coefficients of CFST columns and FRP-confined concrete columns. Therefore, they introduced the following formula for calculating the stability load bearing capacity of FCFST immediate long columns.

$$N_{ul} = \varphi_s N_s + \varphi_f N_f \tag{3}$$

$$\varphi_s = 0.115\sqrt{L/D-4} \tag{4}$$

$$\varphi_f = 0.0013(\frac{L}{D})^2 - 0.067(\frac{L}{D}) + 1.08 \tag{5}$$

where N_{ul} is the axial-compressed ultimate load bearing capacity of FCFST immediate long columns; φ_s is the stability coefficient for CFST columns; φ_f is the stability coefficient for FRP-confined concrete columns; N_s is the ultimate load bearing capacity of CFST short columns; N_f is the ultimate load bearing capacity of FRP-confined concrete short columns; L is the column length; D is the cross-sectional diameter of the component. The specific calculation method is detailed in literature [26].

Wang et al. [27] defined slenderness ratio limit values for FCFST short, immediate long and long columns. They proposed stability coefficient calculation formulas as follows:

$$N_{ul} = \varphi N_{us} \tag{6}$$

$$\varphi = \begin{cases} 1 & \lambda \le \lambda_0 \\ a\lambda^2 + b\lambda + c & \lambda_0 < \lambda \le \lambda_p \\ d/(\lambda+35)^2 & \lambda > \lambda_p \end{cases} \tag{7}$$

where N_{ul} is the axial-compressed ultimate load bearing capacity of FCFST columns; φ is the stability coefficient; λ_0 is the slenderness ratio limit for short and immediate long columns; λ_p is the slenderness ratio limit for immediate long columns and long columns; a, b, c, and d are respective calculation parameters; N_{us} is the axial-compressed ultimate load bearing capacity of FCFST short columns. The specific calculation method is detailed in literature [27].

Shen et al. [28] derived the formula for calculating the ultimate load bearing capacity of FCFST short columns based on literature [29]. Combining it with the stability coefficient method, they obtained the formula for calculating the axial-compressed ultimate load bearing capacity of FCFST immediate long columns as follows:

$$N_{ul} = \varphi N_{us} \tag{8}$$

$$\varphi = \frac{1}{2\overline{\lambda_{csc}}^2}\left[\overline{\lambda_{csc}}^2 + (1+0.25\overline{\lambda_{csc}}) - \sqrt{(\overline{\lambda_{csc}}^2 + (1+0.25\overline{\lambda_{csc}}))^2 - 4\overline{\lambda_{csc}}^2}\right] \tag{9}$$

where N_{ul} is the axial-compressed ultimate load bearing capacity of FCFST immediate long columns; φ is the stability coefficient; N_{us} is the axial-compressed ultimate load bearing capacity of FCFST short columns; $\overline{\lambda_{csc}}$ is the normalized slenderness ratio of the component. The specific calculation method is detailed in literature [28].

To assess the accuracy and applicability of the aforementioned models, experimental data from this study were input into these models to obtain ultimate load bearing capacity theoretical values N_{ulc}. A comparison was made with the experimental values N_{ule}, then using three key metrics: the average value of N_{ulc}/N_{ule} (AV), standard deviation (SD), and average absolute error (AAE), to evaluate data dispersion. The calculation methods for these three metrics are as follows:

$$AV = \frac{\sum_{i=1}^{n}(N_{ulc}/N_{ule})}{n} \tag{10}$$

$$SD = \sqrt{\frac{1}{n}\sum_{i=1}^{n}(N_{ulc}/N_{ule} - A)^2} \tag{11}$$

$$AAE = \frac{1}{n}\sum\left|\frac{N_{ulc} - N_{ule}}{N_{ule}}\right| \quad (12)$$

Table 4 presents a comparison of the theoretical calculation values and experimental values for the ultimate load bearing capacity of specimens in this study. From the table, it is evident that the Yu et al. [26] model has an AV and AAE of 0.59 and 0.41, respectively. It indicates an underestimation of the ultimate load bearing capacity of FCTSSC immediate long columns, with a significant error. Wang et al. [27] model has an AV and SD of 1.48 and 0.30, respectively. It overly considers the restraining effect of FRP, resulting in an overestimation of the ultimate load bearing capacity of FCTSSC immediate long columns, with a high level of prediction variability. Shen et al. [28] model predictions are slightly on the higher side, while Liu et al. [25] model exhibits higher prediction accuracy, with an AV and AAE of only 1.01 and 0.06, respectively. It can offer better predictions for the ultimate load bearing capacity of FCTSSC immediate long columns. There is limited existing research on FCTSSC immediate long columns, so it lacks systematic and representative studies. Overall, the existing models are still insufficient for accurately predicting the ultimate load bearing capacity of FCTSSC immediate long columns. Therefore, further analysis is required to get the differences in the restraint provided by inner and outer FRP fabric layers, as well as to discuss the impact laws of more parameters. Then proposing a more accurate and applicable theoretical model for predicting the ultimate load bearing capacity of FCTSSC immediate long columns.

Table 4 *Assessment result of previous models*

Load Bearing Model	Specimen Identification	N_{ulc}	N_{ule}	N_{ulc}/N_{ule}	AV	SD	AAE
Liu et al. [25]	CF1SC24	1866.71	2032.53	0.92	1.01	0.08	0.06
	CF2SC24	2154.12	2151.29	1.00			
	CF3SC24	2417.05	2183.68	1.11			
Yu et al. [26]	CF1SC24	995.06	2032.53	0.49	0.59	0.08	0.41
	CF2SC24	1249.97	2151.29	0.58			
	CF3SC24	1505.87	2183.68	0.69			
Wang et al. [27]	CF1SC24	2269.05	2032.53	1.12	1.48	0.30	0.48
	CF2SC24	3144.75	2151.29	1.46			
	CF3SC24	4029.65	2183.68	1.85			
Shen et al. [28]	CF1SC24	2161.58	2032.53	1.06	1.17	0.09	0.17
	CF2SC24	2488.38	2151.29	1.16			
	CF3SC24	2796.42	2183.68	1.28			

5. Conclusion

A novel type of FCTSSC intermediate long column that has not been previously researched. Axial compression tests were conducted on these columns with different numbers of external CFRP layers. The following conclusions can be drawn:

- When FCTSSC intermediate long column specimens reach their ultimate load bearing capacity, there is an instantaneous rupture of the local CFRP fabric. Subsequently, the surface of the steel tube in that area gradually bulges. Eventually, the specimens exhibit a failure mode of global buckling accompanied by local steel tube expansion.
- Compared to SFST specimens, FCTSSC intermediate long column specimens displayed an increase in ultimate load bearing capacity ranging from 12.51% to 20.87%. Furthermore, their ultimate load bearing capacity and enhancement percentage were positively correlated with the external CFRP layers number.
- As the external CFRP layers number increases, the efficiency of CFRP confinement gradually decreases. Hence, it is recommended that in practical engineering applications, FCTSSC intermediate long column specimens should employ two layers of external CFRP fabric for more economical and rational usage.
- FCTSSC intermediate long column specimens exhibited good ductility. The peak lateral deformation is positively correlated with the external CFRP layers number. The peak lateral deformation ranges at 2/4 and 3/4 heights were 5.62 mm to 6.31 mm and 6.21 mm to 7.75 mm, respectively. Notably, lateral deformations at 3/4 height were consistently greater than those at 2/4 height.
- In the existing load bearing capacity models, the Yu et al. [26] model underestimates the ultimate load bearing capacity of FCTSSC immediate long columns. Models from Wang et al. [27] and Shen et al. [28] overpredict the values, while the Liu et al. [25] model exhibits higher prediction accuracy.
- For this study, Liu et al. [25] model can be used to predict the ultimate bearing capacity of FCTSSC intermediate long column. However, due to the limited research and insufficient experimental data currently

available, more studies are needed in the future to develop a more representative and comprehensive bearing capacity model.

Acknowledgement

The authors gratefully acknowledge the financial support for this research received from the Universiti Teknologi Malaysia (RMC) Grant No. [Q.J130000.5022.10G22].

Conflict of Interest

Authors declare that there is no conflict of interests regarding the publication of the paper.

Author Contribution

The authors confirm contribution to the paper as follows: ***study conception and design:*** *Hao Fu, Chee-Loong Chin;* ***data collection:*** *Hao Fu, Kangle Guo, Zhaojun Wu;* ***analysis and interpretation of results:*** *Hao Fu, Rihao Mai, Chau-Khun Ma;* ***draft manuscript preparation:*** *Hao Fu, Chee-Loong Chin. All authors reviewed the results and approved the final version of the manuscript.*

References

[1] Xiao, J., Qiang, C., Nanni, A., & Zhang, K. (2017). Use of sea-sand and seawater in concrete construction: Current status and future opportunities. Construction and Building Materials, 155, 1101-1111. https://doi.org/10.1016/j.conbuildmat.2017.08.130

[2] Zhou, A., Qin, R., Feo, L., Penna, R., & Lau, D. (2017). Investigation on interfacial defect criticality of FRP-bonded concrete beams. Composites Part B: Engineering, 113, 80-90. https://doi.org/10.1016/j.compositesb.2016.12.055

[3] Liao, J., Zeng, J.-J., Bai, Y.-L., & Zhang, L. (2022). Bond strength of GFRP bars to high strength and ultra-high strength fiber reinforced seawater sea-sand concrete (SSC). Composite Structures, 281, 115013. https://doi.org/10.1016/j.compstruct.2021.115013

[4] Zeng, J.-J., Zhuge, Y., Liang, S.-D., Bai, Y.-L., Liao, J., & Zhang, L. (2022). Durability assessment of PEN/PET FRP composites based on accelerated aging in alkaline solution/seawater with different temperatures. Construction and Building Materials, 327, 126992. https://doi.org/10.1016/j.conbuildmat.2022.126992

[5] Zeng, J.-J., Gao, W.-Y., Duan, Z.-J., Bai, Y.-L., Guo, Y.-C., & Ouyang, L.-J. (2020). Axial compressive behavior of polyethylene terephthalate/carbon FRP-confined seawater sea-sand concrete in circular columns. Construction and Building Materials, 234, 117383. https://doi.org/10.1016/j.conbuildmat.2019.117383

[6] Fu, H., Zhang, J., Wu, Z., Chin, C.-L., & Ma, C.-K. (2023). Nonlinear analysis of axial-compressed corroded circular steel pipes reinforced by FRP-casing grouting. Journal of Constructional Steel Research, 201, 107689. https://doi.org/10.1016/j.jcsr.2022.107689

[7] Ostrowski, K., Dudek, M., & Sadowski, Ł. (2020). Compressive behaviour of concrete-filled carbon fiber-reinforced polymer steel composite tube columns made of high performance concrete. Composite Structures, 234, 111668. https://doi.org/10.1016/j.compstruct.2019.111668

[8] Zeng, J.-J., Guo, Y.-C., Liao, J., Shi, S.-W., Bai, Y.-L., & Zhang, L. (2022). Behavior of hybrid PET FRP confined concrete-filled high-strength steel tube columns under eccentric compression. Case Studies in Construction Materials, 16, e00967. https://doi.org/10.1016/j.cscm.2022.e00967

[9] Fu, H., Zhao, H., Pan, Z., Wu, Z., Chin, C.-L., & Ma, C.-K. (2023). Behaviour of corroded circular steel tube strengthened with external FRP tube grouting under eccentric loading: Numerical study. Structures, 56, 104810. https://doi.org/10.1016/j.istruc.2023.06.141

[10] Teng, J. G., Yu, T., Dai, J. G., & Chen, G. M. (2011). FRP composites in new construction: Current status and opportunities. The 7th National Conference on FRP Composition, Industrial Construction, pp. 179-186

[11] Li, Y. L., Zhao, X. L., Raman Singh, R. K., & Al-Saadi, S. (2016). Tests on seawater and sea sand concrete-filled CFRP, BFRP and stainless steel tubular stub columns. Thin-Walled Structures, 108, 163-184. https://doi.org/10.1016/j.tws.2016.08.016

[12] Li, Y. L., Teng, J. G., Zhao, X. L., & Singh Raman, R. K. (2018). Theoretical model for seawater and sea sand concrete-filled circular FRP tubular stub columns under axial compression. Engineering Structures, 160, 71-84. https://doi.org/10.1016/j.engstruct.2018.01.017

[13] Bazli, M., Li, Y.-L., Zhao, X.-L., Raman, R. K. S., Bai, Y., Al-Saadi, S., & Haque, A. (2020). Durability of seawater and sea sand concrete filled filament wound FRP tubes under seawater environments. Composites Part B: Engineering, 202, 108409. https://doi.org/10.1016/j.compositesb.2020.108409

[14] Li, S., Guo, S., Yao, Y., Jin, Z., Shi, C., & Zhu, D. (2021). The effects of aging in seawater and SWSSC and strain rate on the tensile performance of GFRP/BFRP composites: A critical review. Construction and Building Materials, 282, 122534. https://doi.org/10.1016/j.conbuildmat.2021.122534

[15] Wang, Z., Zhao, X.-L., Xian, G., Wu, G., Singh Raman, R. K., Al-Saadi, S., & Haque, A. (2017). Long-term durability of basalt- and glass-fibre reinforced polymer (BFRP/GFRP) bars in seawater and sea sand concrete environment. Construction and Building Materials, 139, 467-489. https://doi.org/10.1016/j.conbuildmat.2017.02.038
[16] Cai, Y., & Kwan, A. K. H. (2021). Behaviour and design of cold-formed austenitic stainless steel circular tubes infilled with seawater sea-sand concrete. Engineering Structures, 241, 112435. https://doi.org/10.1016/j.engstruct.2021.112435
[17] Liao, F.-Y., Hou, C., Zhang, W.-J., & Ren, J. (2019). Experimental investigation on sea sand concrete-filled stainless steel tubular stub columns. Journal of Constructional Steel Research, 155, 46-61. https://doi.org/10.1016/j.jcsr.2018.12.009
[18] Zhang, Y., Wei, Y., Bai, J., Wu, G., & Dong, Z. (2020). A novel seawater and sea sand concrete filled FRP-carbon steel composite tube column: Concept and behaviour. Composite Structures, 246, 112421. https://doi.org/10.1016/j.compstruct.2020.112421
[19] Wei, Y., Bai, J., Zhang, Y., Miao, K., & Zheng, K. (2021). Compressive performance of high-strength seawater and sea sand concrete-filled circular FRP-steel composite tube columns. Engineering Structures, 240, 112357. https://doi.org/10.1016/j.engstruct.2021.112357
[20] Wang, G., Wei, Y., Miao, K., Dong, F., & Zheng, K. (2022). Experimental study on axial compression performance of CFRP-steel composite tube filled circular seawater sea-sand coral concrete columns. Acta Materiae Compositae Sinica, 39(8), 3982-3993. http://dx.doi.org/10.13801/j.cnki.fhclxb.20210909.012
[21] Zhang, Y., Wei, Y., Miao, K., & Li, B. (2022). A novel seawater and sea sand concrete-filled FRP-carbon steel composite tube column: Cyclic axial compression behaviour and modelling. Engineering Structures, 252, 113531. https://doi.org/10.1016/j.engstruct.2021.113531
[22] Huang, G., Lin, Y., & Kang, H. (2023). Axial compression test of CFRP-steel pipe-CFRP composite steel pipe confined sea sand concrete short columns. Journal of Fuzhou University, 51(02), 171-177.
[23] JGJ 55-2011 (2011). Specification for mix proportion design of ordinary concrete. Ministry of Housing and Urban-Rural Development, People's Republic of China.
[24] ASTM D1141-98 (2013). Standard Practice for the Preparation of Substitute Ocean Water. ASTM International, United States.
[25] Liu, L. (2009). Research on the basic mechanical properties of FRP and concrete-filled steel tube composite columns. Thesis, Wuhan University.
[26] Yu, F., & Wu, P. (2011). Research on the bearing capacity of FRP-constrained concrete-filled steel tube long columns. FRP/Composites, 4, 60-62.
[27] Wang, Q. L., Qu, S. E., Shao, Y. B., & Feng, L. M. (2016). Static behavior of axially compressed circular concrete filled cfrp-steel tubular (c-cf-cfrp-st) columns with moderate slenderness ratio. Advanced Steel Construction, 12(3), 33. http://dx.doi.org/10.18057/IJASC.2016.12.3.4
[28] Shen, Y. (2022). Analysis of axial compression stability of CFRP round concrete filled steel tube medium and long columns. Thesis, Harbin Engineering University.
[29] Sun, G., & Gu, W. (2017). Simplified analysis of bearing capacity of CFRP-confined concrete-filled steel tube core columns. Journal of Water Conservancy and Construction Engineering, 15(4), 74-78.